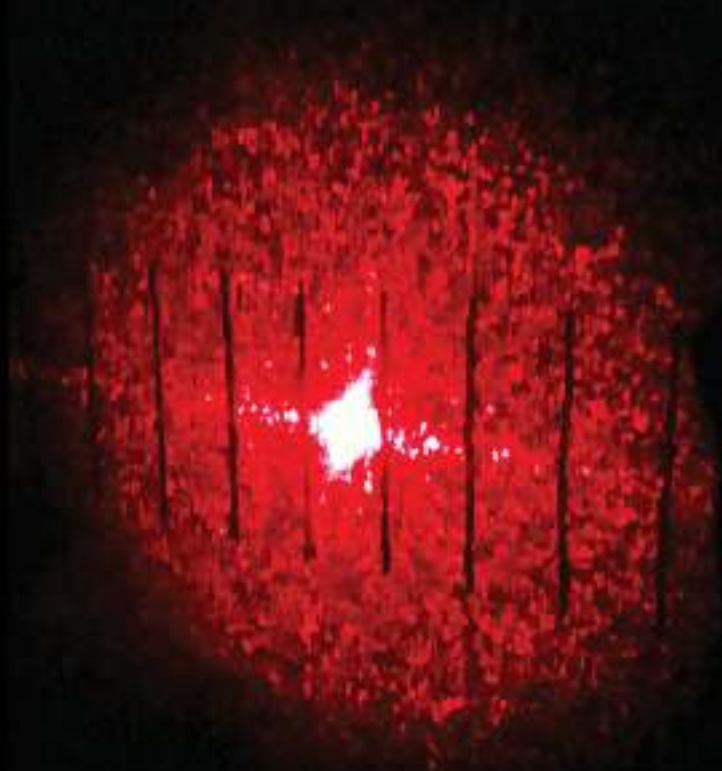


Random Light Beams

Theory and Applications



Olga Korotkova

 CRC Press
Taylor & Francis Group

Random Light Beams

Theory and Applications

Random Light Beams

Theory and Applications

Olga Korotkova



CRC Press
Taylor & Francis Group
Boca Raton London New York

CRC Press is an imprint of the
Taylor & Francis Group, an **informa** business

CRC Press
Taylor & Francis Group
6000 Broken Sound Parkway NW, Suite 300
Boca Raton, FL 33487-2742

© 2014 by Taylor & Francis Group, LLC
CRC Press is an imprint of Taylor & Francis Group, an Informa business

No claim to original U.S. Government works
Version Date: 20130725

International Standard Book Number-13: 978-1-4398-1951-7 (eBook - PDF)

This book contains information obtained from authentic and highly regarded sources. Reasonable efforts have been made to publish reliable data and information, but the author and publisher cannot assume responsibility for the validity of all materials or the consequences of their use. The authors and publishers have attempted to trace the copyright holders of all material reproduced in this publication and apologize to copyright holders if permission to publish in this form has not been obtained. If any copyright material has not been acknowledged please write and let us know so we may rectify in any future reprint.

Except as permitted under U.S. Copyright Law, no part of this book may be reprinted, reproduced, transmitted, or utilized in any form by any electronic, mechanical, or other means, now known or hereafter invented, including photocopying, microfilming, and recording, or in any information storage or retrieval system, without written permission from the publishers.

For permission to photocopy or use material electronically from this work, please access www.copyright.com (<http://www.copyright.com/>) or contact the Copyright Clearance Center, Inc. (CCC), 222 Rosewood Drive, Danvers, MA 01923, 978-750-8400. CCC is a not-for-profit organization that provides licenses and registration for a variety of users. For organizations that have been granted a photocopy license by the CCC, a separate system of payment has been arranged.

Trademark Notice: Product or corporate names may be trademarks or registered trademarks, and are used only for identification and explanation without intent to infringe.

Visit the Taylor & Francis Web site at
<http://www.taylorandfrancis.com>

and the CRC Press Web site at
<http://www.crcpress.com>

Contents

1	Introduction	1
1.1	Brief history	1
1.2	Preliminary mathematics	4
1.2.1	Random processes	4
1.2.2	Spectral representation of random processes	7
1.2.3	Analytic representation of complex signals	10
1.2.4	Gaussian random processes	11
1.3	Preliminary optics	12
1.3.1	Maxwell's, wave and Helmholtz equations	12
1.3.2	Angular spectrum representation and beam conditions	15
1.3.3	Exact beams	19
1.3.3.1	Plane waves and cosine beams	20
1.3.3.2	Bessel beams	22
1.3.3.3	Mathieu beams	24
1.3.3.4	Parabolic beams	25
1.3.4	Vectorial nature of optical fields: polarization	28
1.3.4.1	Polarization ellipse	28
1.3.4.2	Jones calculus	29
1.3.4.3	Stokes vectors	31
1.3.5	Spatial interference in light fields	33
	Bibliography	35
2	Deterministic paraxial beams	39
2.1	Basic family of Gaussian beams	39
2.1.1	Fundamental Gaussian beam	40
2.1.2	Hermite-Gaussian beams	46
2.1.3	Laguerre-Gaussian beams	47
2.2	Superposition of Gaussian beams	50
2.2.1	Flat-top beams	50
2.2.2	Cusp-Gaussian beams	54
2.2.3	Dark-hollow beams	57
2.3	Other deterministic beams	59
	Bibliography	61

3	Scalar stochastic beams: theory	65
3.1	Statistical description	65
3.1.1	Mutual coherence function	66
3.1.2	Cross-spectral density function	67
3.1.3	Spectral and coherence properties	69
3.1.4	Total, encircled and fractional power	70
3.1.5	Higher-order statistical properties	71
3.1.6	Coherent mode decomposition	72
3.1.7	Angular spectrum decomposition	74
3.2	Mathematical models	77
3.2.1	General structure	77
3.2.2	Gaussian Schell-model sources	79
3.2.3	J_0 -Bessel correlated sources	87
3.2.4	Multi-Gaussian correlated sources	93
3.2.5	Bessel-Gaussian-correlated and Laguerre-Gaussian-correlated Schell-model sources	100
3.2.6	Non-uniformly correlated sources	104
3.2.7	I_0 -Bessel correlated sources	108
3.3	Methods of generation	113
	Bibliography	119
4	Electromagnetic stochastic beams: theory	123
4.1	Statistical description	123
4.1.1	Beam coherence polarization matrix	123
4.1.2	Cross-spectral density matrix	124
4.1.3	Spectral, coherence and polarization properties	126
4.1.4	Classic and generalized Stokes parameters	130
4.1.5	Coherent mode decomposition	132
4.1.6	Angular-spectrum decomposition	134
4.2	Electromagnetic quasi-homogeneous sources	138
4.2.1	Far-field analysis and the reciprocity relations	138
4.2.2	Conditions for spectral invariance	142
4.2.3	Conditions for polarization invariance	143
4.3	Propagation in free space and linear media	146
4.3.1	Propagation in free space	146
4.3.2	Conservation laws for electromagnetic stochastic free fields	147
4.3.3	Propagation in linear deterministic media with arbitrary index of refraction	151
4.4	Generalized Jones-Mueller calculus	152
4.4.1	Transmission through deterministic devices	152
4.4.2	Transmission through random devices	157
4.4.3	Combination of several devices	157
4.5	Electromagnetic Gaussian Schell-model sources and beams	159

4.5.1	Realizability and beam conditions	159
4.5.2	Methods of generation	165
4.5.3	Propagation in free space	168
4.6	Electromagnetic beams with Gaussian statistics	170
4.6.1	Higher-order statistical moments of fields	170
4.6.2	Higher-order moments of beams with Gaussian statistics	175
4.6.3	Fluctuations in power	176
4.6.4	Higher-order moments of Stokes parameters	179
4.7	Other stochastic electromagnetic beams	185
4.7.1	Electromagnetic multi-Gaussian Schell-model beams	185
4.7.2	Electromagnetic non-uniformly correlated beams	188
Bibliography		195
5	Interaction of random electromagnetic beams with optical systems	201
5.1	<i>ABCD</i> matrix method for beam interaction with image-forming optical systems	201
5.2	Random beams in the human eye	207
5.3	Random beams in negative phase materials	213
5.4	Imaging by twisted random beams	219
5.5	Tensor method for random beam interaction with astigmatic <i>ABCD</i> systems	225
5.6	Electromagnetic random beams in optical resonators	227
Bibliography		233
6	Random beams in linear random media	237
6.1	Natural random media: turbulence	237
6.1.1	Atmospheric turbulence	239
6.1.2	Oceanic turbulence	242
6.1.3	Biological tissues	243
6.2	Scalar random beam interaction with random media	246
6.2.1	Extended Huygens-Fresnel principle	247
6.2.2	Angular spectrum method	250
6.2.3	Fractional power changes	254
6.2.4	Correlation-induced spectral changes	255
6.3	Electromagnetic random beam interaction with random media	263
6.3.1	General theory	263
6.3.2	Polarization changes in random media	264
6.3.3	Propagation in non-Kolmogorov atmospheric turbulence	267
6.3.4	Propagation in oceanic turbulence	272
Bibliography		279

7	Mitigation of random media effects with random beams	285
7.1	Free-space optical communications	285
7.1.1	Communication link quality criteria	286
7.1.2	The pdf models for beam intensity in the atmosphere	288
7.2	Mitigation of scintillations by different randomization schemes	292
7.2.1	Non-uniform polarization	292
7.2.2	Partial coherence	295
7.2.3	Combination of non-uniform polarization and partial coherence	296
7.3	Active LIDAR systems with rough targets	299
7.3.1	Beam propagation in optical systems in the presence of random medium	300
7.3.2	Beam passage through a LIDAR system with a semi-rough target	302
7.3.3	Target characterization: inverse problem	311
	Bibliography	315
8	Weak scattering of random beams	319
8.1	Classic theory of weak scattering	319
8.2	Description of scattering media	322
8.2.1	Single scatterer	322
8.2.2	Collections of scatterers	326
8.2.3	Random scatterers	326
8.3	Weak scattering for scalar fields	327
8.3.1	Cross-spectral density function of scattered field . . .	327
8.3.2	Coherence effects on Mie scattering	332
8.3.3	Scattering from turbulent medium containing particles	333
8.4	Weak scattering of electromagnetic fields	335
8.4.1	Cross-spectral density matrix of scattered field	335
8.4.2	Scattering from a delta-correlated slab	341
8.4.3	Scattering from a thin bio-tissue layer	344
	Bibliography	351
	Index	355

List of Figures

1.1	Intensity distributions in transverse cross-sections of typical stochastic beams produced with the help of the spatial light modulator. (left) random beam with flat-top intensity profile; (right) ring-shaped beam.	2
1.2	Simulated transverse cross-sections of a typical stochastic beam (left) at 10 m and (right) at 50 m from the source.	3
1.3	Illustration of realizations of a random process.	5
1.4	Notation relating to beam propagation.	18
1.5	McCutchen sphere.	21
1.6	The density plots of the transverse intensity distributions of J_0 -Bessel beam (left) and J_1 -Bessel beam (right) with $k_{\perp}=1$	24
1.7	Longitudinal (top) and transverse (bottom, left) intensity distributions of a typical Mathieu beam; angular spectrum (bottom, right), from Ref. [28].	25
1.8	Longitudinal (top) and transverse (bottom, left) intensity distributions of a typical parabolic beam; phase distribution (bottom, right), from Ref. [30].	27
1.9	Polarization ellipse of a monochromatic optical field.	29
1.10	Poincaré sphere.	32
1.11	Young's interference experiment.	33
2.1	Parameters of a Gaussian beam.	45
2.2	Intensity distributions of typical circular (left) and elliptical (right) Gaussian beams, as functions of x and y [m], at $z = 0$, with $w_0 = 1$ cm.	45
2.3	Intensity distributions of several first beams in the Hermite-Gaussian family as functions of x and y , [m], at $z = 0$, with $w_0 = 1$ cm.	48
2.4	Intensity distributions of several first beams in the Laguerre-Gaussian family as functions of x/w_0 and y/w_0 , at $z = 0$	51
2.5	Intensity distributions of typical multi-Gaussian beams as functions of ρ/w_0 , $M = 1, 3, 40$	53
2.6	Two-dimensional intensity distributions of the typical multi-Gaussian beams as functions of ρ/w_{0x} and ρ/w_{0y} , $N = M = 10$	54
2.7	Intensity distributions of several cusp-Gaussian beams as functions of ρ/w_0 , $M = 1, 3, 40$	55

2.8	Typical two-dimensional intensity distributions of cusp-Gaussian beams with different geometries, as functions of x/w_{0x} and y/w_{0y} , $N = M = 10$	56
2.9	Intensity distributions of dark-hollow Gaussian beams as functions of ρ/w_0 , $N = 1, 3, 40$	58
2.10	Intensity distributions of two-dimensional dark-hollow Gaussian beams as functions of x/w_{0x} and y/w_{0y} , $N = M = 10$	58
3.1	The mutual coherence function of the beam is obtained on correlating the fields $V(\mathbf{r}_1)$ and $V(\mathbf{r}_2)$ over a long time interval.	66
3.2	Notation relating to propagation of stochastic beams.	75
3.3	Illustrating a scalar quasi-homogeneous source.	78
3.4	The degree of coherence of the Gaussian Schell-model source as a function of separation distance $\rho'_d = \boldsymbol{\rho}'_2 - \boldsymbol{\rho}'_1 $ for several values of parameter δ : $\delta = 0.01$ mm (dotted curve), $\delta = 0.1$ mm (dashed curve) and $\delta = 1$ mm (solid curve).	80
3.5	The spectral density of a Gaussian Schell-model beam with $\sigma = 1$ cm and $\lambda = 628 \mu\text{m}$ as a function of ρ [m]. (left) At $z = 100$ m from the source plane for several values of parameter δ : $\delta = 0.5$ mm (dotted curve), $\delta = 0.1$ mm (dashed curve) and $\delta = 0.05$ mm (solid curve). (right) With $\delta = 0.1$ mm for several propagation distances: $z = 0$ m (dotted curve), $z = 50$ m (dashed curve), $z = 100$ m (dot-dashed curve), $z = 150$ m (solid curve).	82
3.6	The modulus of the spectral degree coherence of a Gaussian Schell-model beam with $\lambda = 628 \mu\text{m}$ and $\sigma = 1$ cm as a function of the half-distance $\rho_d/2$ [m] between two points $\boldsymbol{\rho}_1 = -\boldsymbol{\rho}_2$. (left) At $z = 100$ m from the source plane for several values of parameter δ : $\delta = 0.1$ mm (dotted curve), $\delta = 0.05$ mm (dashed curve) and $\delta = 0.01$ mm (solid curve). (right) With $\delta = 0.1$ mm for several propagation distances: $z = 0$ m (dotted curve), $z = 10$ m (dashed curve), $z = 50$ m (dot-dashed curve), $z = 100$ m (solid curve).	83
3.7	The contours of the fractional power in transverse cross-sections of a Gaussian Schell-model beam with $\lambda = 0.632 \mu\text{m}$, $\sigma = 1$ cm. (top) $\delta \gg \sigma$ (almost coherent source); (middle) $\delta = 0.1\sigma$ (partially coherent source); (bottom) $\delta \ll \sigma$ (nearly incoherent source). The beam is captured by a circular aperture with radius $\bar{\rho}$. From Ref. [11].	84
3.8	Spectral shift of a typical Gaussian Schell-model beam with a Gaussian spectral profile propagating in free space; $\lambda_{0I} = 0.5 \mu\text{m}$, $\Lambda_I = 0.1 \mu\text{m}$, $\sigma = 1$ mm, $\delta = 0.1$ mm, $z = 0$ (solid curve), $z = 1$ m (dashed curve), $z = 2$ m (dotted curve) and $z = 100$ m (dash-dotted curve).	84

- 3.9 Spectral shifts of two Gaussian Schell-model beams with different r.m.s. widths of correlation coefficients, $\delta(\lambda)$, with a Gaussian spectral profile propagating in free space. Left top figure: $\delta(\lambda)$: $\lambda_{0\delta} = 0.4 \mu\text{m}$ (solid curve); $\lambda_{0\delta} = 0.8 \mu\text{m}$ (dashed curve). The rest of the figures: evolution of beams with two $\delta(\lambda)$ in left top figure in space. The other parameters of two beams are $\lambda_{0I} = 0.4 \mu\text{m}$, $\Lambda_I = \Lambda_\delta = \lambda_{0I}/4$, $\sigma_0 = 1 \text{ cm}$, $\delta_0 = 1 \text{ mm}$ 86
- 3.10 The spectral degree of coherence of the J_0 -Bessel correlated source μ_m as a function of separation distance $\rho'_d = |\boldsymbol{\rho}'_1 - \boldsymbol{\rho}'_2|$ [mm] for several values of parameter β : $\beta = 0.1$ (dotted curve), $\beta = 1$ (dashed curve) and $\beta = 10$ (solid curve). 88
- 3.11 Spectral density profiles of the J_0 -correlated Schell-model beam as a function of the normalized radius ρ/w_0 at several normalized distances: $z/z_R = 0$ (dotted curve), $z/z_R = 0.5$ (dashed curve), $z/z_R = 1$ (solid curve). (left) $\beta w_0/2 = 10$; (right) $\beta w_0/2 = 0.1$ 92
- 3.12 The modulus of the spectral degree of coherence of the J_0 -correlated Schell-model beam as a function of the separation distance ρ'_d at several normalized distances: at several normalized distances: $z/z_R = 0$ (dotted curve), $z/z_R = 0.2$ (dashed curve), $z/z_R = 1$ (solid curve). (left) $\beta w_0/2 = 10$; (right) $\beta w_0/2 = 0.1$ 92
- 3.13 (left) The degree of coherence $\mu^{(MG)}$ for several values of M ; (right) Far-field spectral density of the field generated by the multi-Gaussian Schell-model source vs. $\theta = \arcsin(u_\perp)$ (radians) for several values of M . From Ref. [44]. 94
- 3.14 Transverse cross-section of the spectral density of the multi-Gaussian Schell-model beam propagating in free space vs. $|\boldsymbol{\rho}|$, at several distances from the source plane: (a) 1 m; (b) 100 m; (c) 1 km; and (d) 10 km; $M = 1$ solid curve, $M = 4$ dashed curve, $M = 10$ dotted curve and $M = 40$ dash-dotted curve. Other beam parameters are: $\lambda = 632 \mu\text{ m}$, $\sigma = 1 \text{ cm}$, $\delta = 1 \text{ mm}$. From Ref. [45]. 98
- 3.15 The modulus of the spectral degree of coherence of the multi-Gaussian Schell-model beam propagating in free space vs. ρ_d , at the same distances from the source, values of M and source parameters as in Fig. 3.14. From Ref [45]. 99
- 3.16 The spectral degree of coherence of (a) the Bessel-Gaussian-correlated sources, (b) the Laguerre-Gaussian-correlated sources. From Ref. [46]. 102
- 3.17 Far field generated by a typical Bessel-Gaussian-correlated source for several values of order n : (a) $\beta_b = 0$, (b) $\beta_b = 2.5$, (c) $\beta_b = 20$. From Ref. [46]. 103

3.18	The far fields generated by typical Laguerre-Gaussian-correlated sources for several values of n : (a) $n = 0$; (b) $n = 1$; (c) $n = 30$. From Ref. [46].	105
3.19	(a) Absolute value of the cross-spectral density and (b) the degree of coherence of a typical beam with non-uniform correlations. The axes correspond to x_1 and x_2 in millimeters and their scale in the insets is the same as in the larger figures. From Ref. [47].	106
3.20	Propagation of a typical beam with non-uniform correlations. Figures on the left side show the evolution of the intensity at the $(x-z)$ plane. On the right side, the lateral intensity distribution is shown at selected propagation distances. The upper row: $\gamma_0 = 0$, the bottom row: $\gamma_0 \neq 0$. From Ref. [47].	107
3.21	Contours of the modulus of the spectral degree of coherence of the I_0 -Bessel correlated source, as function of $x = \rho'_1/\delta_I$ and $y = \rho'_2/\delta_I$. (left) $n = 0$; (right) $n = 10$	110
3.22	Contours of the modulus of the spectral degree of coherence of the stochastic I_0 -Bessel correlated beam, as a function of $x = \rho_1/\delta_I$ and $y = \rho_2/\delta_I$. (a) $n = 0$, $z/z_R = 1$; (b) $n = 0$, $z/z_R = 10$; (c) $m = 10$, $z/z_R = 1$; (d) $m = 10$, $z/z_R = 10$	112
3.23	Spatial Light Modulator.	114
3.24	Typical realizations of the SLM phase screens for the Gaussian Schell-model beams with different correlation widths.	116
3.25	Comparison of the SLM phase screen realizations for Schell-model sources: (left) Gaussian; (middle) Bessel-Gaussian; (right) Laguerre-Gaussian. From Ref. [46].	117
4.1	Fluctuating in time electric vector field at two spatial positions \mathbf{r}_1 and \mathbf{r}_2	124
4.2	Illustration of the concept of an electromagnetic quasi-homogeneous source.	139
4.3	Transmission of a deterministic field through a thin device of polarization optics.	154
4.4	Transmission of a random beam through a thin device of polarization optics.	154
4.5	Cascaded system of linear non-image-forming devices.	158
4.6	Optical arrangements for producing electromagnetic Gaussian Schell-model beams: (a) from Ref. [57]; (b) from Ref. [58].	167
4.7	Evolution of the polarization properties of a typical electromagnetic Gaussian Schell-model beam propagating in free space. From Ref. [12]. Different curves corresponds to different sets of the r.m.s. widths of correlation functions δ_{xx} , δ_{xy} and δ_{yy}	171
4.8	Evolution of the Stokes parameters of the polarization ellipse of a typical electromagnetic Gaussian Schell-model beam propagating in free space. From Ref. [20].	172

4.9	Spectral changes of electromagnetic Gaussian Schell-model beams generated by sources with several different coherence and polarization states, and propagating in free space. Subfigures show the source degree of coherence. Curves: 1 — source; 2 — $\theta = 0^\circ$; 3 — $\theta = 0.3^\circ$. From Ref. [32].	173
4.10	Contour plots of intensity (left) and contrasts (right) of the Gaussian Schell-model beam with Gaussian statistics. From Ref. [62].	177
4.11	Changes in the contrast of the intensity of the Gaussian Schell-model beam with Gaussian statistics. From Ref. [62].	178
4.12	The changes in the probability density functions of the instantaneous Stokes parameters of a typical random beam: (a) pdf[$S_0(\rho = 0, z)$], (b) pdf[$S_1(\rho = 0, z)$], (c) pdf[$S_2(\rho = 0, z)$] and (d) pdf[$S_3(\rho = 0, z)$] at several distances z from the source. From Ref. [69].	183
4.13	The changes in the probability density functions of the normalized instantaneous Stokes parameters of a typical random beam: (a) pdf[$s_1(\rho = 0, z)$], (b) pdf[$s_2(\rho = 0, z)$], (c) pdf[$s_3(\rho = 0, z)$] at several distances z from the source. From Ref. [69].	184
4.14	Changes in the polarization ellipse associated with the polarized part of the electromagnetic multi-Gaussian Schell-model beams for different values of index M (left $M = 1$), (right $M = 30$). From Ref. [75].	189
4.15	Spectral density of the propagating electromagnetic non-uniformly correlated beam in a transverse plane $z = 30$ m. (a) $\boldsymbol{\gamma}_x = (0.8\sigma_0, 0)$, $\boldsymbol{\gamma}_y = (0.9\sigma_0, 0)$ and (b) $\boldsymbol{\gamma}_x = (0.8\sigma_0, 0)$, $\boldsymbol{\gamma}_y = (-0.9\sigma_0, 0)$. From Ref. [76].	192
4.16	Distribution of the degree of polarization of the beam in transverse planes: (a) $z = 0$ m, (b) $z = 1$ m; (c) $z = 15$ m; (d) $z = 30$ m. From Ref. [77].	193
5.1	Aligned optical elements.	202
5.2	Diagram representing $ABCD$ matrix approach for optical systems with Gaussian lenses.	204
5.3	Optical fibers: (a) step-index fiber; (b) GRIN fiber.	205
5.4	Contour plots of the refractive index distribution of the crystalline lens.	207
5.5	Illustration of notations used for beam propagation in the human eye. From Ref. [18].	209
5.6	Contour plots of actual spectral shift λ_1 overlapped with contour plots of normalized spectral shift $\varrho = \frac{\lambda_1 - \lambda_0}{\lambda_0}$ as a function of $z + d$ (horizontal axis) and ρ (vertical axis); (top) crystalline lens; (bottom) free space.	211

5.7	(left) The spectral density $S(\rho, z + d; \omega)$; (right) The spectral degree of polarization $\wp(\rho, z + d; \omega)$ of the beam vs. propagation distance z [m] after the lens for: coherent beam, $\delta_{xx} = \delta_{yy} = \delta_{xy} = \delta_{yx} \rightarrow \infty$ (solid curve); partially coherent beam $\delta_{xx} = \delta_{yy} = 1.125 \times 10^{-4}$ m (dotted curve), $\delta_{xy} = \delta_{yx} = 1.25 \times 10^{-4}$ m, nearly incoherent beam $\delta_{xx} = \delta_{yy} = 1.125 \times 10^{-5}$ m, $\delta_{xy} = \delta_{yx} = 1.25 \times 10^{-5}$ m (dashed curve). From Ref. [18].	213
5.8	The spectral density (intensity) of the beam (on-axis) as a function of propagation distance z from the source. From Ref. [26].	216
5.9	The degree of coherence of the beam at two points with separation distance $\rho_d = 10^{-5}$ m as a function of propagation distance z from the source. From Ref. [26].	217
5.10	The degree of polarization of the beam (on-axis) as a function of propagation distance z from the source. From Ref. [26]. . .	217
5.11	Spectral changes in Gaussian Schell-model beams on propagation in layers of PPM and NPM. From Ref. [27].	218
5.12	Spectral changes of Gaussian Schell-model beams on propagation in layers of PPM and NPM with absorption. From Ref [27].	219
5.13	A two-lens imaging system.	220
5.14	Image of two illuminated pinholes, plotted in normalized coordinates, for different phases ϕ_t . The other parameters are: $\delta = 0.1$ mm, $\lambda = 0.59$ μ m, $R = 1$ cm, $f = 0.5$ m, $\sigma = 1$ mm, $d = 0.61\lambda f/R$, $y_0 = 5$ mm. From Ref. [34].	222
5.15	Image of two illuminated pinholes, plotted in normalized coordinates, for different values of coherence width δ , with $\phi_t = \pi$, $d = 0.24\lambda f/R$. The rest of the parameters are as in Fig. 5.14. From Ref. [34].	224
5.16	Contour image of two pinholes with completely incoherent illuminating source (left) and partially coherent illuminating source $\delta = 0.1$ mm (right) with $d = 0.213\lambda f R$. The rest of the parameters are as in Fig. 5.14. From Ref. [34].	224
5.17	A typical laser cavity: (a) Actual arrangement; (b) Unfolded version.	228
5.18	On-axis degree of polarization versus number of passages N for different values of cavity parameter g_R and the source correlation coefficients. m_1 : $\delta_{xx} = \delta_{yy} = 0.1$ mm, $\delta_{xy} = \delta_{yx} = 0.2$ mm; m_2 : $\delta_{xx} = \delta_{yy} = 0.25$ mm, $\delta_{xy} = \delta_{yx} = 0.5$ mm; m_3 : $\delta_{xx} = \delta_{yy} = 0.5$ mm, $\delta_{xy} = \delta_{yx} = 1$ mm. From Ref. [51]. . . .	229
5.19	On-axis degree of polarization versus N for different values of mirror spot size ϵ_R in a Gaussian plane-parallel cavity ($g_R = 1$) with $\delta_{xx} = \delta_{yy} = 0.1$ mm, $\delta_{xy} = \delta_{yx} = 0.2$ mm. From Ref. [51].	230
5.20	On-axis degree of polarization versus N for different values of g_R in a lossless cavity ($\epsilon_R \rightarrow \infty$) with $\delta_{xx} = \delta_{yy} = 0.1$ mm, $\delta_{xy} = \delta_{yx} = 0.2$ mm. From Ref. [51].	231

5.21	The degree of polarization versus one transversal dimension x for different values of the mirror spot size and the source correlation coefficients in a Gaussian plane-parallel cavity ($g_R = 1$). m_1 , m_2 and m_3 take the same values as in Fig. 5.18. From Ref. [51].	231
6.1	Turbulent cascade.	239
6.2	Non-Kolmogorov atmospheric turbulence: three-layered model. Solid and dashed curves refer to two different data fits. From Ref. [18].	241
6.3	Computer simulation of turbulent phase screens for $\alpha = 3.10$ (left) and $\alpha = 3.67$ (right).	242
6.4	Log-log plot of the oceanic power spectrum $\Phi_n(\kappa)$, calculated from Eqs. (6.15)-(6.16) and normalized by the Kolmogorov power-law $\kappa^{-11/3}$, for $w_K = -0.1$ (solid curve), $w_K = -2.5$ (dotted curve), $w_K = -4.9$ (dashed curve). From Ref. [23].	244
6.5	The structure of the mouse liver tissue power spectrum in the logarithmic scale. From Ref. [25].	244
6.6	Illustrating notations relating to beam propagation in turbulence.	248
6.7	Radial distribution of the spectral density of a Bessel beam propagating in atmospheric turbulence. From Ref. [36].	254
6.8	Radial distribution of the spectral density (intensity) of a Gaussian beam (left) and a Gaussian Schell-model beam (right) propagating in free space (dash-dotted curves) and in atmospheric turbulence (solid and dashed curves) with the von Karman power spectrum, at different distances z from the source. From Ref. [36].	255
6.9	Contours of the fractional power in cross-sections of a Gaussian Schell-model beam with $\lambda = 0.633 \mu\text{m}$, $\sigma = 1\text{ cm}$, on propagation in turbulent atmosphere with Kolmogorov power spectrum and $C_n^2 = 10^{-13}\text{ m}^{-2/3}$: almost coherent source (top), partially coherent source with $\delta/\sigma = 0.1$ (middle) and nearly incoherent source (bottom). From Ref. [38].	256
6.10	The normalized spectral density \mathcal{S}_N [unitless] of a random beam propagating in atmospheric turbulence as a function of λ for $\rho = 0$ and different α : $\alpha = 3.01$ (dashed curve), $\alpha = 3.1$ (dotted curve), $\alpha = 3.67$ (dot-dashed curve) and free space (solid, thin curve), at $z = 0.5\text{ km}$, $z = 1\text{ km}$, and $z = 5\text{ km}$. Solid thick curve shows the normalized spectral density in the source plane. From Ref. [58].	258

- 6.11 Contour plots of normalized spectral shift $\varrho_\lambda = \frac{\lambda_1 - \lambda_0}{\lambda_0}$ of a random beam propagating in atmospheric turbulence as a function of z (horizontal axis, in meters) and ρ (vertical axis, in meters) for (a) $\alpha = 3.01$; (b) $\alpha = 3.10$, (c) $\alpha = 3.67$; (d) free space. From Ref. [58]. 259
- 6.12 Contour plots of the normalized spectral shift $\varrho_\lambda = \frac{\lambda_1 - \lambda_0}{\lambda_0}$ of a random beam propagating in atmospheric turbulence as a function of z (horizontal axis, in meters) and α (vertical axis) for $\rho = 0$ (on the beam axis). 260
- 6.13 Contour plots of normalized spectral shift $\varrho_\lambda = \frac{\lambda_1 - \lambda_0}{\lambda_0}$ as a function of z (horizontal axis, in meters) and ρ (vertical axis, in meters) for (a) $\chi_T = 10^{-10} K^2/s$; (b) $\chi_T = 10^{-5} K^2/s$, (c) $\chi_T = 10^{-4} K^2/s$; (d) $\chi_T = 10^{-2} K^2/s$; $\varepsilon_K = 10^{-4} m^2/s^3$, $w_K = -4.5$. From Ref. [23]. 261
- 6.14 Contour plots of normalized spectral shift $\varrho_\lambda = \frac{\lambda_1 - \lambda_0}{\lambda_0}$ as a function of z (horizontal axis, in meters) and (a) χ_T , on a log scale for $\varepsilon_K = 10^{-4} m^2/s^3$, $w_K = -2.5$, (b) w_K for $\varepsilon_K = 10^{-4} m^2/s^3$, $\chi_T = 10^{-4.5} K^2/s$, (c) ε_K , on a log scale (vertical axis) for $\chi_T = 10^{-4.5} K^2/s$, $w_K = -2.5$; $\rho = 0$. From Ref. [23]. . . 262
- 6.15 Propagation of the polarization ellipse of the electromagnetic Gaussian Schell-model beam along the optical axis. From Ref. [74]. 268
- 6.16 Comparison of the polarization properties of a typical electromagnetic Gaussian Schell-model beam on propagation in free space and in turbulent atmosphere. From Ref. [74]. 269
- 6.17 Propagation of the degree of polarization along the optical axis of the beam produced by an electromagnetic Gaussian Schell-model source with (a) uniform polarization; (b) non-uniform polarization. The Kolmogorov model for the power spectrum was used to characterize the atmospheric fluctuations, values of structure parameter are given for each curve in $m^{-2/3}$. Curves in (a) illustrate the recovery effect of the degree of polarization at large propagation distances from the source. From Ref. [80]. 270
- 6.18 The normalized spectral density S_N and the spectral degree of polarization \wp as functions of α for $\rho = 0$, $z = 1$ km, $A_x = 1$. From Ref. [77]. 271
- 6.19 (left) The normalized spectral density S_N and (right) the spectral degree of polarization \wp as functions of distance z for $\rho = 0$, $A_x = 1$, and different α : $\alpha = 3.01$ (solid curve), $\alpha = 3.1$ (dashed curve), $\alpha = 3.67$ (dotted curve) and free space (dot-dashed curve) on a log scale. From Ref. [77]. 272

6.20	(left) The absolute value of the spectral degree of coherence as a function of distance z for $\rho = 10^{-3}$ m, $A_x = 1.3$ and different α : $\alpha = 3.01$ (solid curve), $\alpha = 3.1$ (dashed curve), $\alpha = 3.67$ (dotted curve) and free space (dot-dashed curve) on a log scale; (right) The absolute value of the spectral degree of coherence as a function of ρ for $z = 1$ km, $A_x = 1.3$ and the same α . From Ref. [77].	273
6.21	Typical evolution of the polarization properties of a stochastic beam in oceanic turbulence (on-axis). From Ref [75].	274
6.22	Variation of the statistical properties of the beam with distance z (horizontal axis, in meters) for several values of the root-mean-square correlation coefficient δ_{xx} of the source. From Ref [75].	275
6.23	Variation of the degree of polarization of the beam with distance z (horizontal axis, in meters) for several values of (a) the mean square temperature dissipation rate χ_T ; (b) the energy dissipation rate per unit mass ε_K ; (c) the temperature-salinity balance parameter w_K . From Ref [75].	276
7.1	Photophone: one of the first devices transforming sound to optical wave. From Ref. [1].	286
7.2	A typical optical communication link.	287
7.3	The probability density function of the normalized intensity reconstructed by the Gamma-Gamma and the Gamma-Laguerre models. (left) Experiment above land; (right) Experiment above water. Dots represent actually measured intensity levels. From Ref. [7].	291
7.4	The probability density function of the normalized intensity of a partially coherent beam beam (left) and a corresponding laser beam (right). Dots represent the data points and the line is produced with the help of the Gamma-Laguerre pdf model.	292
7.5	Simulation of the scintillation index of the non-uniformly polarized beam propagating at 5 km in the turbulent atmosphere of the two Laguerre-Gaussian modes as a function of (left) the amplitude ratio; (right) the Rytov variance. From Ref. [8].	294
7.6	Simulation of the intensity and polarization state of a non-uniformly polarized beam in atmospheric turbulence. Density plot (gray scale) shows distribution of intensity along the major axis of polarization, x and, lines - polarization state in: (a) the source plane, $z = 0$, (b) in the field $z = 5$ km. From Ref. [8].	294
7.7	The scintillation index of a scalar Gaussian Schell-model beam with $\sigma = 1$ cm propagating in the turbulent atmosphere versus the Rytov variance σ_R^2	296

7.8	Evolution of the on-axis scintillation index of two Gaussian Schell-model beams: (a) linearly polarized, (b) unpolarized, in atmospheric turbulence as a function of the Rytov variance: (left) weak turbulence, (right) moderate and strong turbulence. From Ref. [18].	298
7.9	Propagation of the scintillation index of three unpolarized electromagnetic Gaussian Schell-model beams as a function of Rytov variance: (a) almost coherent source; (b) partially coherent source, (c) almost incoherent source. (left) Weak theory, (right) moderate and strong theory. From Ref. [18].	298
7.10	(top) Bistatic LIDAR system; (bottom) unfolded version of bistatic LIDAR system.	304
7.11	The spectral density (left column) and the spectral degree of polarization (right column) at the source plane (top), at the target plane (middle) and at the collecting lens plane (bottom). From Ref. [35].	309
7.12	The spectral degree of polarization at the collecting lens plane for several values of roughness parameter: (A) $\delta_T = 0.05$ mm, (B) $\delta_T = 0.1$ mm, (C) $\delta_T = 0.5$ mm, (D) $\delta_T = 1$ mm. From Ref. [35].	310
8.1	Illustrating the notation of scattering theory. From Ref. [5].	320
8.2	Illustrating scattering to the far field. From Ref. [5].	322
8.3	Illustrating the notation relating to an ellipsoid. From Ref. [7].	324
8.4	Illustrating three basic rotations defining the orientation of the particle frame $[\xi, \eta, \zeta]$ relative to the laboratory frame $[x, y, z]$. From Ref. [7].	324
8.5	Scattering potential for solid particles (left) and hollow particles (right) as a function of $r/(\sqrt{2}\sigma)$ for several values of M : $M = 1$ (dashed-dotted curve); $M = 4$ (dashed curve); $M = 10$, (dotted curve) and $M = 40$ (solid thick curve). From Ref. [7].	326
8.6	Normalized angular distribution of the radiant intensity generated by scattering of partially coherent beams by a hard sphere. From Ref. [19].	333
8.7	Illustrating the notation relating the incident field propagating to the scatterer. From Ref. [2].	336
8.8	Illustrating the spherical coordinate system and notation relating the scatterer and the scattered field in the far zone. From Ref. [2].	338
8.9	(a) The normalized spectral density of the scattered field in the far zone vs. the inclination angle, with $\phi = \frac{\pi}{6}$; (b) The spectral degree of polarization of the scattered field in the far zone vs. the inclination angle, with $\phi = 0$. From Ref [2].	344

8.10	The spectral degree of coherence of the scattered field in the far zone at two points vs. the azimuthal separation angle. From Ref. [2].	345
8.11	Scattering from thin tissue layer. From Ref. [44].	347
8.12	The spectral degree of polarization scattered from a tissue as a function of azimuthal angle θ : for different types of tissues (left); for different correlation properties of the incident beam (right). From Ref. [44].	349

Foreword

“..... I'd gladly be locked up in a dungeon ten fathoms below ground, if in return I could find out one thing: What is light?”

Galileo Galilei

I wrote this book during my first several years of professorship at the Department of Physics of the University of Miami, FL. Being heavily involved in the research topics discussed in this text since the time of my dissertation, I recently started to realize that certain subtleties that at some point seemed to have transparent explanations could readily escape from memory. My own need for this monograph became apparent. It also was so for my group of graduate and undergraduate students as well as visiting scholars. Even if technically it is not my first book (my Ph.D. thesis has recently been published in Germany), I perceive it as being such. It is also dearer to me since while working on this text I have discovered tons of facts in areas of optics that I had thought before I knew well. Moreover, it was a remarkable revelation that namely the author of the book seems to learn more than everybody else from it. By no means is this text designed as a self-sufficient account of classical statistical optics. It is only meant to be an upgrade for a particular direction, the one relating to various phenomena associated with beam-like fields which are random in nature.

In Chapter 1 the essential mathematical and physical concepts needed for deeper understanding of the main text are reviewed. Various classes of deterministic paraxial beams are introduced in Chapter 2. Some of these beams are used in subsequent chapters as building blocks for random beams. Chapter 3 concerns random scalar beams, which were explored in depth several decades ago and discussed in detail in other books, for instance, the fundamental text *Optical Coherence and Quantum Optics* by L. Mandel and E. Wolf and *Coherent Mode Representation in Optics* by A. Ostrovsky. Hence, we will only briefly present the well-established issues relating to scalar beams and focus on the findings not yet reflected in the literature. In Chapter 4 we introduce electromagnetic random beams and point out the matters relating to their generation, propagation in free space and various media, transmission through optical systems, etc. Some of this analysis can be found in a fairly new book titled *Introduction to the Theories of Coherence and Polarization of Light* by E. Wolf. This book, however, treats a greater variety of aspects and goes deeper into details. Chapters 5 to 8 discuss some of the applications that benefit from the use of random beams. In particular, in Chapter 5 the interac-

tion of beams with deterministic optical systems is explored and the examples are given of light propagation through the human eye, laser resonators, negative phase materials, etc. Chapters 6 and 7 are concerned with propagation of random beams in random media, such as the atmosphere and ocean, as well as with optical systems operating in their presence. Finally, Chapter 8 is devoted to scattering of random beams from collections of scatterers and thin random layers, such as bio-tissue slices.

While being the sole author of this monograph I am indebted to my advisors, colleagues and students who through both short in-office discussions and profound e-mail correspondence stimulated my interest in this diverse and fast-growing field. At times entire articles of my graduate students N. Farwell, S. Sahin, and Z. Tong were used as book sections and uncountable number of times their comments and ideas were included. I am particularly grateful for the financial support of our research group provided in recent years by the US Air Force Research Office (A. Nachman, K. Miller), the US Office of Naval Research (R. Malek-Madani) and also by the Physics Department and College of Arts and Sciences at the University of Miami. The last but not least acknowledgment goes to my colleagues and co-authors of more than a hundred peer-reviewed papers including Y. Cai, G. Gbur, F. Gori, D. Zhao, J. Pu, E. Wolf, L. Andrews, R. Phillips, Y. Baykal, S. Avramov-Zamurovic, C. Nelson, E. Shchepakina, Z. Mei and many others for their perpetual guidance and shared insight into statistical optics, mathematical modeling and optical engineering.

Olga Korotkova
January 2013

- [download online The Smashing Book #3: Redesign the Web](#)
- [read How the Fox Got His Color - CÃ³mo el zorro obtuvo su color \(English-Spanish Bilingual Edition\) pdf, azw \(kindle\), epub, doc, mobi](#)
- [click The Adventures of Nick Mane, Private Detective - Mind's Eye pdf, azw \(kindle\), epub](#)
- [read online The Bone Bed \(Kay Scarpetta, Book 20\) pdf](#)
- [click Favorite Design Challenges pdf](#)
- [Environmental Management Accounting for Cleaner Production \(Eco-Efficiency in Industry and Science\) pdf](#)

- <http://academialanguagebar.com/?ebooks/Antarktos-Rising---A-Novel.pdf>
- <http://cavalldecartro.highlandagency.es/library/DB2-10-5-with-BLU-Acceleration--New-Dynamic-In-Memory-Analytics-for-the-Era-of-Big-Data.pdf>
- <http://nexson.arzamaszev.com/library/Calculus-for-Cognitive-Scientists--Partial-Differential-Equation-Models--Cognitive-Science-and-Technology-.pdf>
- <http://www.experienceolvera.co.uk/library/The-Bone-Bed--Kay-Scarpetta--Book-20-.pdf>
- <http://musor.ruspb.info/?library/Favorite-Design-Challenges.pdf>
- <http://thermco.pl/library/Entrepreneurship--A-Very-Short-Introduction--Very-Short-Introductions-.pdf>